Chapter 15

INTERPLANETARY RADIO BURSTS

N. Gopalswamy
Laboratory for Extraterrestrial Physics NASA/GSFC, Greenbelt, MD

Abstract Nonthermal radio bursts in the interplanetary medium indicate the far-reaching effect of solar eruptions that inject energetic particles, plasmas and shock waves into the inner heliosphere. More than half a century of ground-based observations and subsequent space-based observations exist on this phenomena. In this paper, I summarize the understanding we have gained on the type III and type II radio bursts, which are indicative of electron beams and shocks, respectively. Observations in the new radio window (1-14 MHz) from Wind/WAVES have not only confirmed previous results, but also led to a number of new discoveries. Availability of simultaneous white light (SOHO) and radio (Wind) observations from the same spatial domain in the near-Sun IP medium is largely responsible for these discoveries on the IP propagation of CMEs, so this paper discusses radio bursts in the context of white light observations. After exploring the origin of normal, complex and storm type III bursts, I discuss the type II bursts and their relation to coronal mass ejections. Finally I discuss some of the recent developments on IP radio emission.

1. Introduction

Nonthermal radio bursts in the interplanetary (IP) medium are caused by energetic electrons from the Sun, which convert part of their energy into electromagnetic radiation via an emission mechanism. How exactly these electrons are accelerated during solar eruptions is not fully understood, and is one of the outstanding issues of solar physics. Most of the long-wavelength radio bursts are due to coherent plasma processes, so the frequency of emission is closely related to the plasma frequency (and hence the plasma density) of the medium through which the electrons propagate. Since the plasma density decreases away from the Sun, the plasma frequency also decreases, so radio emission at longer wavelengths originate at greater distances from the Sun. For example, radio emission at metric wavelengths originates close to the Sun, while

D.E. Gary and C.U. Keller (eds.), Solar and Space Weather Radiophysics, 305–333.
© 2004 *Kluwer Academic Publishers. Printed in the Netherlands.*

the kilometric radio emission comes from IP medium close to 1 AU. A proper understanding of the radio bursts can provide useful information about the solar source (where electrons are accelerated) and the IP medium (through which the accelerated electrons propagate).

The day-time peak of the ionospheric electron density is a few times 10^5 cm^{-3}, which corresponds to a plasma frequency of several MHz. Radio emission from the Sun at longer decametric and kilometric wavelengths cannot penetrate the ionosphere, so we must go to space to observe such radiation. Coronal densities similar to the ionospheric densities occur at a heliocentric distance of $\sim 3R_\odot$. The approximate location of the upper source surface of the solar magnetic field is supposed to be near this distance. The ambient medium beyond the source surface may be considered to be that of IP space. In general, therefore, ground based radio telescopes typically access coronal radio emission below the source surface, whereas space based ones must be used to detect radio emission from IP space. Plasma levels at frequencies > 10 MHz are considered coronal, and the lower-frequency levels are taken as IP. Figure 15.1 shows a plot of the level of IP radio emission as compared to the quiet Sun and cosmic background emissions. While the quiet Sun radio emission is very small compared to the galactic background, the solar radio bursts are brighter by several orders of magnitude and hence can be detected easily.

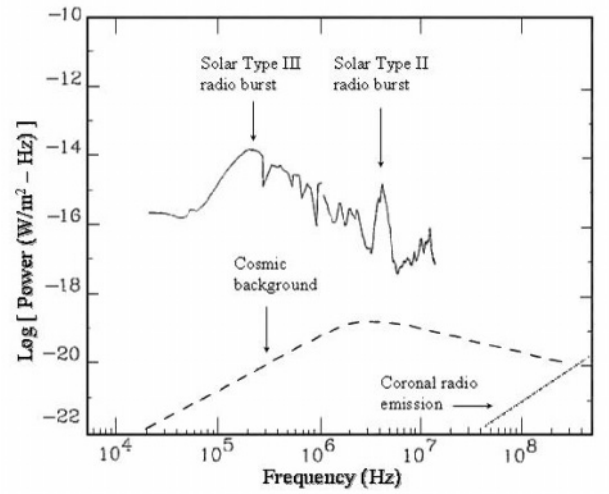

Figure 15.1. Plot showing the level of IP radio burst (types II and III) flux as compared to the cosmic background noise and the quiet coronal emission. The low-frequency end of the solid curve represents *in-situ* plasma frequency. The high-frequency end corresponds to the ionospheric cut-off.

Coronal radio emission has been observed extensively with a variety of ground-based instruments since its discovery by Hey in 1942 but the IP ra-

dio observations became possible only in the space era. The radio instruments on board the Alouette-I satellite observed type III bursts in the 1–8 MHz range and it was possible to infer electron beams with speeds in the range 0.1–0.15c (where c is the speed of light, Hartz 1964). Type II bursts were first identified from IMP-6 data and then from Voyager 2 data (Boischot *et al.* 1980). Extensive observations of coronal mass ejections (CMEs), which became available in the ISEE-3 era, helped enormously in understanding the relationship among shocks, CMEs, and electron beams. Unfortunately, many of the later radio instruments operated at frequencies below 2 MHz, which made it difficult to connect the phenomena observed by ground-based and space-based instruments. The launch of the Wind spacecraft in 1994 essentially closed the gap because the Radio and Plasma Wave (WAVES, Bougeret *et al.* 1995) experiment has a larger frequency range (20 kHz–14 MHz). The spatial domain corresponding to the high-frequency (1–14 MHz) WAVES receiver (RAD2) overlaps with the field of view of the Solar and Heliospheric Observatory (SOHO) mission's Large Angle and Spectrometric Coronagraph (LASCO, Brueckner *et al.* 1995). This synergism has led to the confirmation of a number of old results and enabled new discoveries. The topics in this chapter are mainly concerned with radio phenomena at frequencies below 14 MHz and their relation to solar disturbances such as CMEs. For details on the basic properties of radio bursts, the readers may consult articles in the monograph by Stone *et al.* (2000).

2. Type III Bursts

Type III bursts were first discovered at metric wavelengths by ground-based telescopes in the frequency range 10 to 500 MHz (Wild, 1950). It was recognized early on that electron beams propagating through the coronal and IP plasma can produce these radio bursts (Ginzburg & Zheleznyakov 1958; Wild & Smerd 1972). A beam-plasma system is unstable to the generation of Langmuir waves, which are high frequency plasma waves at the local plasma frequency. Langmuir waves scattered off of ions or low-frequency turbulence result in radiation at the fundamental of the local plasma frequency. Two Langmuir waves can also coalesce to produce electromagnetic waves at twice the local plasma frequency, commonly known as second harmonic emission.

In a dynamic spectrum, the type III bursts appear as almost vertical features because of the high drift rate from high to low frequencies. Since the corona and the IP medium are essentially magnetized plasmas, propagation of electrons occur along open magnetic field lines. Thus, type III bursts continuing from the corona into the IP medium are indicative of open magnetic field lines emanating from the vicinity of the acceleration region and extending into the IP medium. In the inner corona, where closed magnetic field lines are common, one observes a couple of variants of type III bursts such as the J and U bursts,

due to electron beams propagating along curved (or closed) field lines. In the inner corona, one often observes type III bursts with reverse drift. The reverse-drift bursts are due to electrons propagating towards the Sun. The reverse-drift bursts are closely associated with hard X-ray bursts because the latter are also produced by electrons precipitating from the corona and stopped by the chromosphere. Direct observation of nonthermal electrons and plasma waves in space, in association with type III bursts, provided the hard evidence for the plasma emission mechanism (Lin *et al.* 1973). The distribution function of these nonthermal electrons indeed demonstrated the generation of Langmuir waves. Since Langmuir waves derive their energy from the nonthermal electrons, the intensity of the radio bursts depends on the nonthermal electron density and energy (Fitzenreiter *et al.* 1976; Dulk *et al.* 1998).

Type III bursts in the IP space were first detected by the radio instruments on Alouette-I and routinely by later space radio experiments such as ISEE-3, Ulysses, Geotail, and Wind (see Hartz 1964; 1969; Hartz & Gradel 1970; Slysh 1967*ab*; Alexander *et al.* 1969; Fainberg & Stone 1970; Bougeret *et al.* 1998). Radio instruments on board the ATS-II satellite and the Venus 2 Probe observed type III bursts in the 0.45–3 MHz range (Alexander *et al.* 1969), and 0.2–2 MHz (Slysh, 1967*ab*), respectively. The Radio Astronomy Explorer (RAE-I), the first dedicated radio astronomy mission, led to a number of advances in studying electron beams as well as inferring the Archimedean spiral structure of the IP magnetic field (e.g., Fainberg & Stone 1970). When more than one radio instrument was available, it became possible to track the type III radio source: using the RAE-2 and IMP-6 observations, Fitzenreiter *et al.* (1977) obtained the north-south structure in the IP magnetic field. Type III bursts in the IP medium can be grouped into three broad classes representing three different situations of electron beam production and propagation: (i) isolated type III bursts from flares and small-scale energy releases, (ii) complex type III bursts during CMEs, and (iii) type III storms. We discuss them in turn in the next three subsections.

2.1 Isolated type III bursts

Isolated type III bursts are the most common type, produced by energetic electrons escaping from small-scale energy release sites on the Sun. The energy release can occur in regions ranging from small bright points to large active regions. Figure 15.2 shows an example of type III bursts in the metric domain with and without IP counterparts (Gopalswamy *et al.* 1998). The initial type III bursts and the type II burst in the metric domain originated from active region (AR) 7817 with heliographic coordinates, N00E49. However, we do not know the origin of the later intense type III bursts that continued into the Wind/WAVES domain. The isolated kilometric type III bursts are known to be closely associated with He^3-rich events (Reames *et al.* 1988), the class of solar

energetic particle (SEP) events now known as "impulsive" events in contrast to the long-duration (high intensity) SEP events, which are not rich in He^3. Investigation of the source regions of these type III bursts in comparison with the solar sources of the hard X-ray bursts (also due to energetic electrons flowing towards the Sun from the acceleration site) is underway by the RHESSI team.

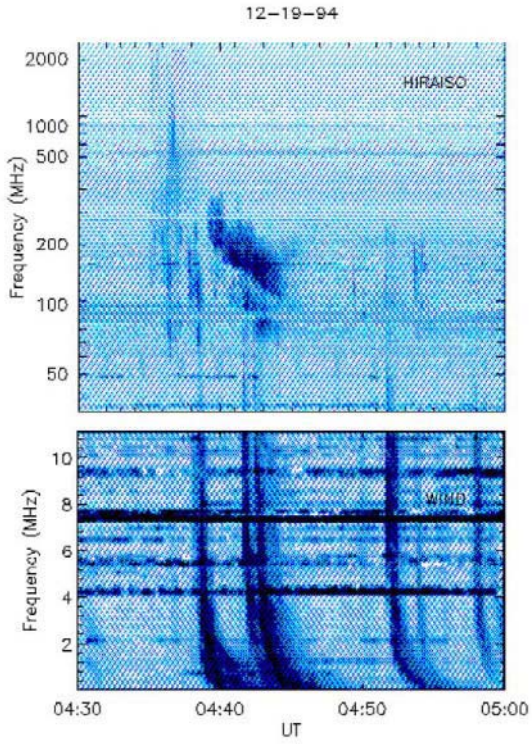

Figure 15.2. A combination of ground-based (Hiraiso; top) and Wind/WAVES (bottom) dynamic spectra showing a number of isolated type III bursts (vertical features). The slanted feature is the type II burst. It is clear that some metric type III bursts continue to lower frequencies, while some do not.

2.2 Complex type III bursts

The complex type III bursts occur in conjunction with CMEs. The bursts were first identified at hectometric wavelengths in the ISEE-3 data (Cane *et al.* 1981) who named them "shock-accelerated" (SA) events. They deduced that the bursts were produced by electron beams accelerated in blast-wave shocks and injected along open magnetic field lines, similar to the herringbone bursts at metric wavelengths. MacDowall *et al.* (1987) introduced a working definition of the SA events: the intensity profile contains five or more peaks of very high intensity

(>100,000 sfu) with an overall duration exceeding 20 min. Figure 15.3 shows an example of the complex type III bursts that occurred on 1997 December 12 from Gopalswamy *et al.* (2000*a*). The event has a group of several bursts in quick succession at high frequencies, which merge to form a single long duration event at lower frequencies.

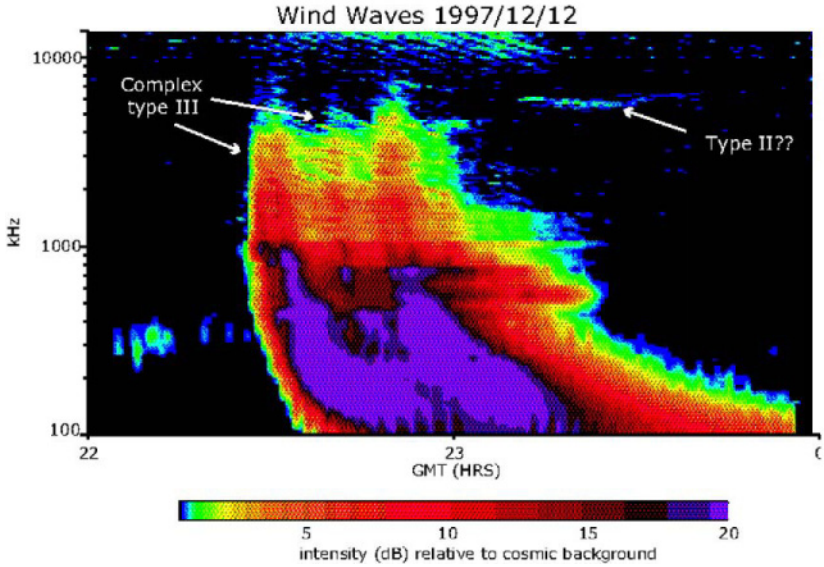

Figure 15.3. The 1997 December 12 complex type III burst that started below about 7 MHz, but was very intense at kilometric wavelengths (from Gopalswamy *et al.* 2000).

2.2.1 Origin of nonthermal electrons. The blast wave origin of the electron acceleration responsible for the complex type III bursts was questioned by Kundu & Stone (1984), who found that the onset times of the complex type III bursts and microwave bursts were identical. These authors concluded that the responsible electrons were accelerated by the common flare process. They also called these bursts "shock-associated" rather than "shock-accelerated" (the acronym SA remained the same!) because of the different origin of the non-thermal electrons. A comparison of SA events with microwave and hard X-ray bursts led Klein (1995) to arrive at similar conclusions. However, Kahler *et al.* (1986) studied a set of metric type II bursts associated with SA events and found that about half of them were not associated with type III bursts in the metric domain, contradicting the low-coronal origin for the SA events. They also found a good association between proton events and SA events, suggesting the involvement of shocks because energetic protons are accelerated by shocks.

Bougeret *et al.* (1998) preferred the term "shock-associated," which could include the possibility that electron beams, accelerated low in the corona, may encounter a shock along their path causing the radio emission to turn on. Reiner *et al.* (2000) noted the similarity in the complexity and duration of the time profiles of 5 complex type III bursts and decimetric (3 GHz) nonthermal emissions, which they presented as further evidence for a flare origin of the electron acceleration. Bougeret et al (1998) showed a complex type III burst, which appeared to start from a metric type II burst with no 3-GHz counterpart. This example is consistent with shock acceleration, unless the decimetric emission was suppressed for some reason. We must point out that relatively smooth decimetric emission, like microwave emission, is due to gyrosynchrotron emission from high energy electrons trapped in closed field lines, while the complex type III bursts are due to low energy electrons propagating along open field lines. Thus the actual duration of decimetric and type III emissions need not agree. One has to compare the lifetime of the trapped particles in closed magnetic field lines with the decay time of plasma waves in the open field region before the time-profile similarity can be used as evidence for the common origin of the nonthermal electrons (Reiner *et al.* 2000). It is not clear if the Reiner *et al.* result would hold for a larger sample of complex type III bursts. Reiner & Kaiser (1999) also argued against the blast-wave origin (Cane *et al.* 1981) for complex type III bursts based on the observation that there are complex type III events without metric type II bursts.

2.2.2 Complex type III bursts and CMEs. In their study of 25 radio-rich CMEs, Gopalswamy *et al.* (2000) found that 23 (92%) of them were associated with SA events (they had incorrectly marked two events—May 2 and 3, 1998—as non-SA events). On the other hand, only half of the SA events associated with front-side CMEs had microwave bursts, while all of them had IP type II bursts. From this they concluded that the presence of CME-driven shocks is essential for the SA events. This clearly brings CMEs into the picture of complex type III bursts. Recently, Cane *et al.* (2002) have changed their interpretation of the SA events to agree with Reiner *et al.* (2000), and have proposed that the electrons are accelerated in reconnection sites behind fast CMEs. However, this does not completely resolve the issue of shock or flare origin, because the presence of fast CMEs also implies the presence of IP shocks near the Sun. In a recent study, MacDowall *et al.* (2003) found that complex type III bursts occurred during almost all large solar energetic particle (SEP) events of solar cycle 23. They also searched for complex type III bursts during impulsive (flare-associated) SEP events and did not find any. Since all large SEP events are associated with fast and wide CMEs with IP type II bursts, the MacDowall *et al.* result also confirms the involvement of CMEs.

The close association between complex type III bursts and shock-driving CMEs (Gopalswamy *et al.* 2000) may have implications for the intensity diminution at 7 MHz, a curious spectral feature reported by Reiner & Kaiser (1999). The intensity diminution has been attributed to complex disturbed magnetic fields around the 7 MHz plasma layer. Not all complex type III bursts show this diminution. Since the associated CMEs are typically fast and wide, one may have to consider the propagation of type III radiation in the presence of high-density CMEs occupying a large volume in the vicinity of complex type III bursts. The CME may affect the propagation of electrons or the propagation of radio waves, depending on where the CME is located with respect to the source of nonthermal electrons and the observer. The magnetically disturbed region invoked by Reiner & Kaiser (1999) may indeed be the associated CME itself.

Irrespective of how the electrons are accelerated (shock or flare site) the occurrence of a CME during the complex type III bursts seems to be required. Figure 15.4 shows the radio dynamic spectrum from Wind/WAVES with the height-time plots of a large number of CMEs on 2000 November 24. Note that all the fast CMEs have associated complex type III bursts. Some CMEs do not have type III association, while some weak type III bursts have no associated CMEs.

In some cases, the complex type III bursts start at much lower frequencies and definitely after the associated type II bursts (Gopalswamy 2000). An example with complex type III bursts starting at lower frequencies after the onset of the metric type II burst is shown in Figure 15.5 (see also Klassen *et al.* 2002). The type II burst was associated with a CME and a filament eruption. The flare in this case was extremely weak and gradual. This event is not inconsistent with electrons accelerated at the shock front and released along open magnetic field lines. The origin of the electrons is thus inconclusive. It is quite possible that both mechanisms could operate to varying degrees.

2.3 Type III storms

Type III storms consist of thousands of short-lived type III-like bursts in rapid succession (Fainberg & Stone 1970; Moller-Pederson 1974). The activity can last for days to weeks. The high frequency counterparts of type III storms are known as "noise storms" or type I storms consisting of narrow-band bursts often superposed on weak continuum emission (see Elgaroy 1977). The storm bursts are thought to be due to electrons from small-scale, quasi-continuous energy releases into closed magnetic structures of active regions. Boishot *et al.* (1970) found a correlation of 80% between type I and decametric type III activity. At coronal heights corresponding to decametric wavelengths, a type I

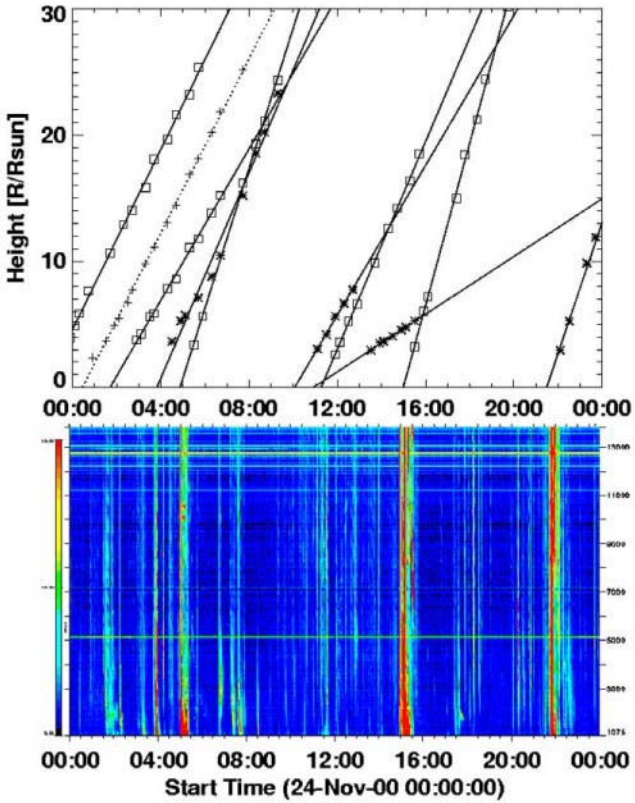

Figure 15.4. Height-time plots of all the CMEs that occurred on 2000 November 24 (top), along with the WAVES/RAD2 dynamic spectrum. Note that all of the complex type III bursts are associated with major CMEs.

storm makes a transition to type III storm (Aubier *et al.* 1978), indicating that electrons gain access to open magnetic field lines of the so-called active region streamers (Stewart & Labrum 1972; Bougeret *et al.* 1984). The occurrence rate of the storm bursts was found to increase as the associated active region crossed the central meridian (Fainberg & Stone 1971). Thus these storms represent energy releases without an eruption of the associated magnetic field structure.

2.3.1 Cessation and recovery of type III storms. What happens when there is an eruption in the active region that has a storm in progress? As one might expect, the type III storms are completely disrupted by large CMEs. After disruption, the type III storms often return to the original level. The cessation and recovery of type III storms may hold the key to understanding how the corona responds to the eruption of large CMEs. Figure 15.6 shows a type III storm during 2000 July 07–08 as observed by Wind/WAVES. On July 07, the

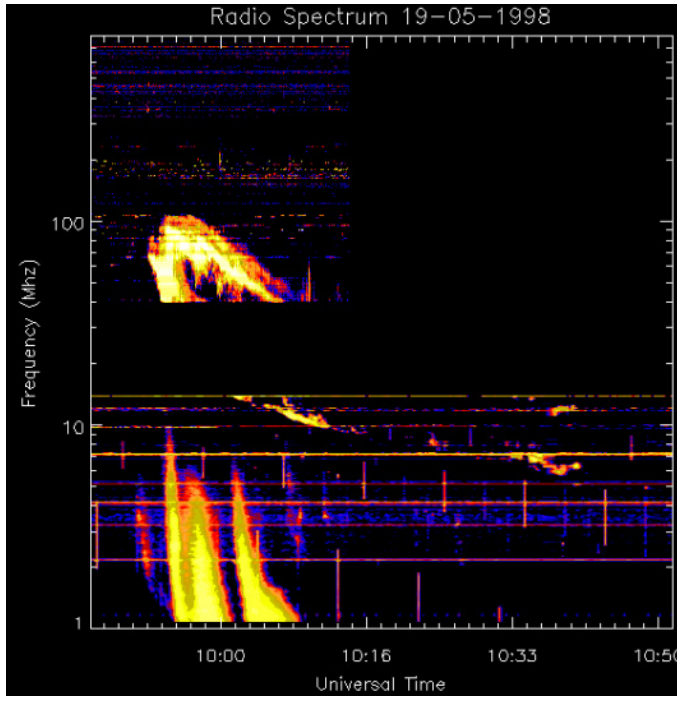

Figure 15.5. A hybrid dynamic spectrum consisting of Potsdam data (top, above 40 MHz) and Wind/WAVES (bottom, below 14 MHz). The Complex type III bursts start only below 10 MHz and delayed with respect to the onset of the type II burst.

storm ceased for about 10 hours from the time of a halo CME from the disk center. The storm came back to its original state by about 20 UT. The storm continued to rage until the end of next day, when there was another CME from the same region and the storm was again interrupted for approximately 8 h. There was also another storm from AR 9077, which continued until the onset of the Bastille Day CME, which disrupted it (see Reiner *et al.* 2001*a*). After the Bastille Day event, the storm recovery took a much longer time of 17 h.

3. Type II Bursts

The slow-drifting radio bursts were first identified by Payne-Scott *et al.* (1947) from the records at 200, 100, and 60 MHz frequencies. The frequency drift was correctly recognized to represent the motion of an exciting agency in the corona, later identified as an MHD shock by Uchida (1960). Wild & McCready (1950) classified the slowly-drifting bursts as type II bursts. These are relatively rare bursts and have been studied extensively at meter-decameter wavelengths using ground based telescopes (see Nelson & Melrose 1985 for a

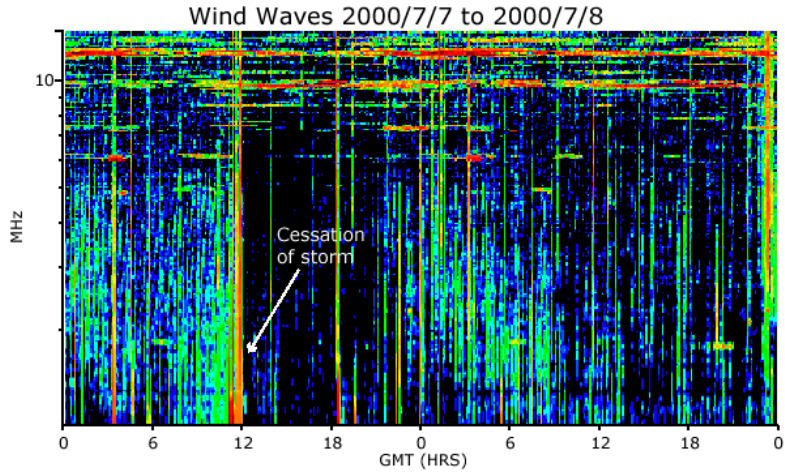

Figure 15.6. Type III storm activity (vertical streaks) observed by Wind/WAVES during 2000 July 7–8. The noise storm was interrupted by a CME on July 7 around 12 UT, but recovers by 20 UT to the original intensity.

review). The current interpretation of the type II burst emission is as follows: electrons accelerated in the MHD shock front generate plasma waves, which get converted into electromagnetic radiation at the fundamental and harmonic of the local plasma frequency.

Type II bursts in the IP medium were first detected by Malitson *et al.* (1973) using IMP 6 data. Voyager data also provided information on IP type II bursts (Boischot *et al.* 1980). The ISEE-3 spacecraft observed about 47 IP type II bursts in the frequency range 30 kHz to 2 MHz over a 50-month period from the L1 point (Lengyel-Frey & Stone 1989). The bursts are intense (up to 1000 sfu at 100 kHz) and have a typical relative bandwidth of 70%. Wind/WAVES data indicates that the IP type II bursts occur more frequently than what ISEE-3 detected. This is likely to be due to the more limited frequency coverage of the ISEE-3 radio instrument (Kaiser, 2003). Figure 15.7 shows an intense IP type II burst extending from 14 MHz down to *in-situ* frequencies (30 KHz). The shock was also detected *in situ* by the WAVES experiment right at the time the type II burst drifts to *in-situ* frequencies ($\sim$20 kHz). The plasma emission process involving electron beams and Langmuir waves (as in the terrestrial electron foreshock and type III radio bursts) was recently verified when Wind spacecraft passed through a type II burst source (Bale *et al.* 1999; Knock *et al.* 2003).

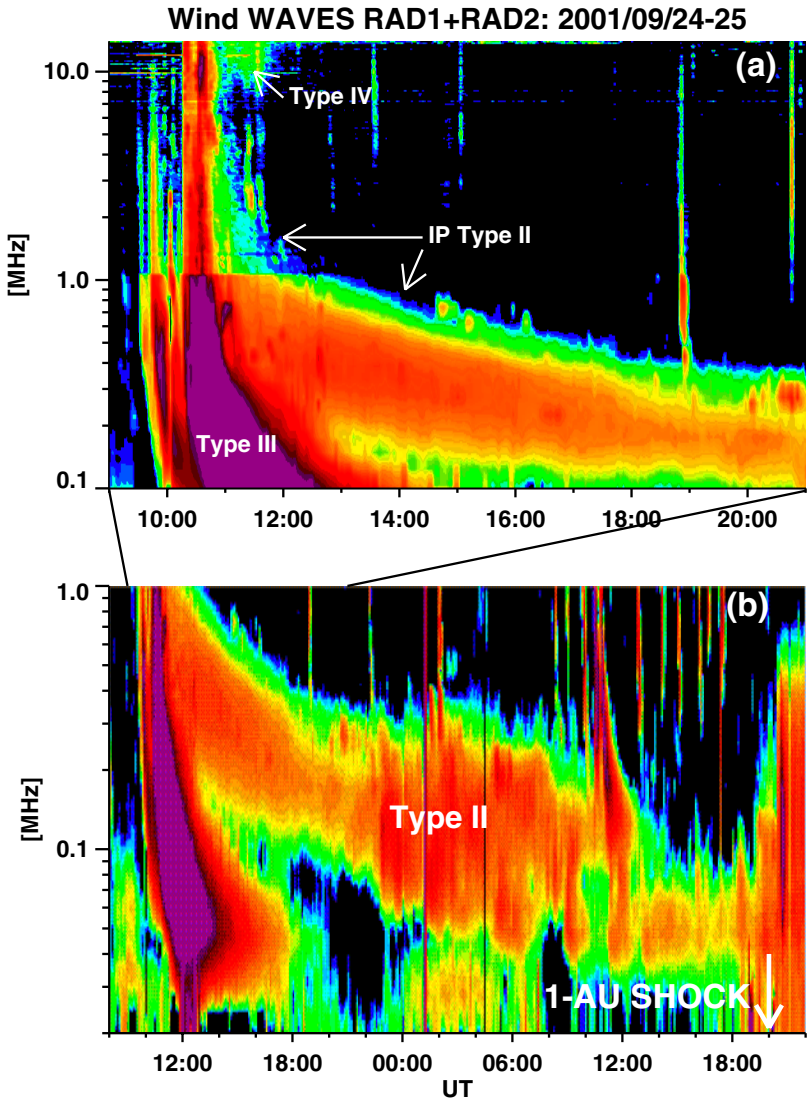

Figure 15.7. IP Type II burst of 2001 September 24-25. The top panel shows the dynamic spectrum over the entire WAVES spectral range. The bottom panel shows the complete evolution of the type II burst until the shock arrived at 1 AU (marked by arrow). The complex Type III, which appeared at the beginning of the event and the associated type IV burst are marked. The collecting area of the antenna in the high-frequency domain is smaller, so the type II burst is faint.

3.1 IP shocks, CMEs and type II radio bursts

The realization that the IP shocks are CME-driven came about when they were found to be closely associated with white-light CMEs (Sheeley *et al.*

1985). At the same time, kilometric type II bursts were also found to be closely associated with IP shocks (Cane *et al.* 1987), so it became clear that the kilometric type II bursts are produced by CME-driven shocks (Cane *et al.* 1987). This confirms the well known *in-situ* observations that many IP shocks are followed by "driver gas" (see, e.g., Borrini *et al.* 1982).

From the inconsistency in the drift rates of type II bursts at frequencies below and above 1 MHz, Cane (1983) concluded that type II bursts above 1 MHz are the continuation of the metric type II bursts and those below 1 MHz are caused by IP shocks. This is consistent with idea of Wagner & MacQueen (1983) that solar eruptions can result in two shocks—a blast wave from the flare and a preceding CME-driven shock due to the CME. According to this idea, the high frequency (metric) type II bursts are caused by the flare shocks (see also Gary *et al.* 1984), while the IP type II bursts are due to CME-driven shocks. Robinson *et al.* (1984) and Cane & Stone (1984) found good correspondence between kilometric type II bursts and metric type II/type IV bursts (70% association), although only 7% of the metric type II bursts were followed by kilometric type II bursts (Robinson *et al.* 1984). Metric type II bursts originate from very close to the solar surface, typically at a height of 0.5 $R_{\odot}$. On the other hand the kilometric type II bursts start beyond 10 $R_{\odot}$. This large gap is a direct result of the lack of frequency coverage between 2 MHz and about 20 MHz.

3.1.1 DH type II bursts. The WAVES/RAD2 frequencies correspond to 2–10 $R_{\odot}$ and hence closed the gap between the kilometric and metric observations. For more than two years after the launch of Wind, no type II bursts were observed in the decametric-hectometric (DH) domain, even though several were observed at metric and kilometric wavelengths (Reiner *et al.* 1998). Gopalswamy *et al.* (1998) noted that none of the 34 metric type II bursts had DH counterparts, but there were IP shocks detected *in situ*. Their analysis also indicated that the IP shocks and metric type II bursts did not come from the same solar source. Starting on 1997 April 01 type II bursts were frequently observed in the DH domain. When Gopalswamy *et al.* (2001a) repeated their study of metric type II bursts and their association with DH and kilometric type II bursts, they found that only 18% and 25% of the metric type II bursts were associated with DH and km type II bursts, respectively. Moreover, 93% of metric type II bursts did not have *in-situ* IP events (shocks or ejecta) and a similar (80%) fraction of IP events had no metric counterparts. Only a small fraction (9%) of metric type II bursts originating from the disk (central meridian distance, CMD $< 60^{\circ}$) were associated with IP shocks; in each of these cases, a halo or partial halo CME was involved (width $> 120^{\circ}$). Thus, even with complete frequency coverage from metric to kilometric wavelengths, the poor correlation between metric and longer wavelength type II bursts was confirmed.

3.2 Are type II bursts CME-driven?

SOHO/LASCO CMEs associated with DH type II bursts had the following properties (see, Gopalswamy *et al.* 2000; 2001*b*): (1) All the DH type II bursts were associated with CMEs. (2) The average speed of the associated CMEs was 1030 km s^{-1}, 2–3 times faster than average CMEs (see Figure 15.8 for the speed distribution of CMEs associated with DH type II bursts). (3) The average width of non-halo CMEs exceeded 100°, nearly twice as wide as the average CMEs. (4) There was a weak correlation between the speed and width of CMEs. (5) The majority (60%) of the CMEs decelerated within the LASCO field of view, with an average value of -11.3 m s^{-2}. (6) The deceleration was proportional to the square of CME speed, as expected when the drag due to the interaction between the ambient medium and the CME becomes important. (7) Only 40% of the fast ($>$ 900 km s^{-1}) CMEs were associated with DH type II bursts.

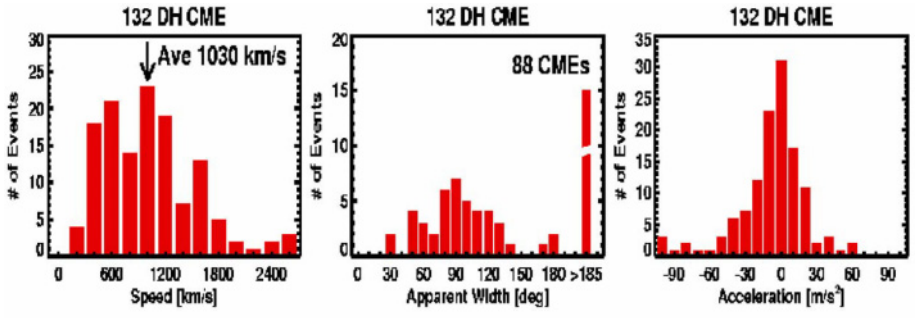

Figure 15.8. Speed, width and acceleration of 132 CMEs associated with DH type II bursts. Note that 88 CMEs were halo events.

A closer examination revealed that fast CMEs without DH type II bursts were not wide; the average width of these CMEs was only 66° as compared to 102° for the ones associated with DH type II bursts (see Figure 15.9). These results prove beyond doubt that DH type II bursts are due to CME-driven shocks, consistent with the high degree of association between kilometric type II bursts and CMEs (see also Kaiser *et al.* 1998; Reiner & Kaiser 1999). It is tempting to extend this association to metric type II bursts also. Gopalswamy *et al.* (2001*a*) reported that a third (34%) of the metric type II bursts originating from the disk were not associated with white light CMEs, as in Kahler *et al.* (1984). However, an EIT wave transient was observed in all these cases, indicating a CME from the disk, probably not observed by the coronagraph by virtue of the solar source location and the nature of coronagraphic observations. This observation supports the conclusion of Cliver *et al.* (1999) that all the metric type II bursts are associated with fast CMEs.

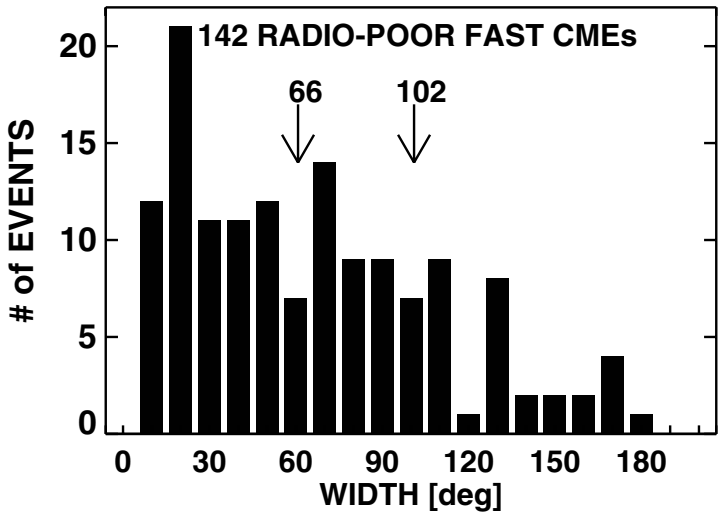

Figure 15.9. Histogram of fast CMEs ($>$ 900 km/s) that did not have associated DH type II bursts. These have an average width of 66°, compared to the 102° for DH type II CMEs.

The close association between DH type II bursts and CMEs on the one hand and the metric type II bursts and CMEs on the other is not consistent with the poor correlation between metric type II bursts and DH type II bursts noted in Gopalswamy *et al.* 2001*b*). Therefore, in addition to the presence of CMEs, additional special conditions need to be satisfied before a metric type II burst can be produced. According to Gosling *et al.* (1976) and Cliver *et al.* (1999) one special condition is a high speed for the CME (fast CMEs). For DH type II bursts, this condition was shown to be fast and wide CMEs (Gopalswamy *et al.* 2001*b*) because 60% of the fast CMEs were radio-poor. In order to see the distinguishing characteristics of CMEs associated with metric type II bursts, Lara *et al.* (2003) considered a set of 80 metric type II bursts that did not have DH counterparts and identified the associated CMEs. They found that the CMEs associated with metric type II bursts are faster (~ 450 km s^{-1}) than the common CMEs (~ 350 km s^{-1}), but they are slower than the CMEs associated with DH type II bursts (see Figure 15.10). The average width of all CMEs ($\sim 50°$) was found to be lower than that ($\sim$70°) for CMEs with metric type II bursts; the latter was, in turn, lower than the average width ($\sim$100°) of CMEs with DH type II bursts. The general population of CMEs had an average acceleration close to zero, while the average had progressively larger negative values for CMEs associated with metric and DH type II bursts. Thus, it appears that type II bursts in all domains are a CME-associated phenomenon.

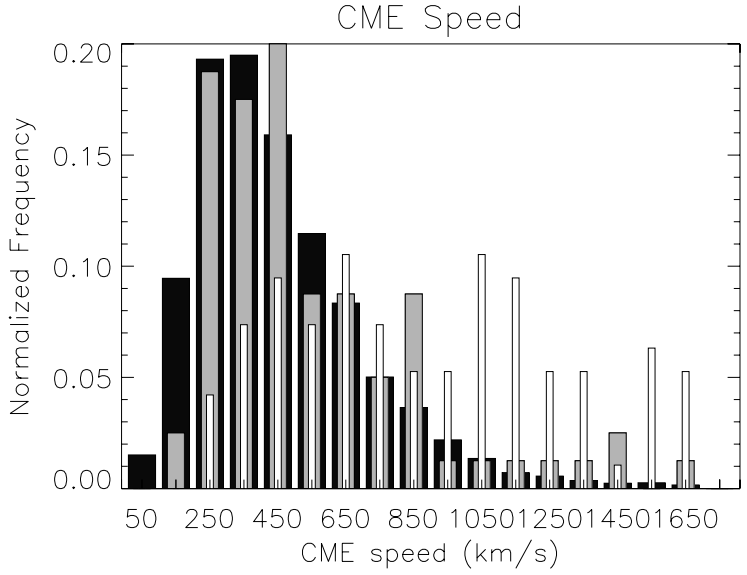

Figure 15.10. Speed distribution of CMEs associated with metric type II bursts as compared to that of general population of CMEs (dark), and DH CMEs (white).

However, there are many fast and wide CMEs without associated DH type II bursts. Gopalswamy *et al.* (2003*b*) investigated a set of fast (> 900 km s^{-1}) and wide (> 60 deg) CMEs that lacked solar energetic particles and DH type II bursts. When they examined the coronagraph images they found that the CMEs were ejected into a tenuous corona. A tenuous corona is expected to have a greater Alfvén speed and hence it is difficult for the CME to drive a shock. Thus the physical properties of the ambient medium such as density and magnetic field (and hence the Alfvén speed) also play a role in deciding the shock-driving capability of CMEs (Uchida *et al.* 1974; Kahler *et al.* 1984), contrary to the conclusion by Cliver *et al.* (1999) that the Alfvén speed is not important.

3.3 What is a fast CME?

In the past, only a single characteristic value was used to define "fast" CMEs: > 400 km s^{-1} (Cliver *et al.* 1999). This number can be traced to Gosling *et al.* (1976) who arrived at the conclusion that, "the characteristic speed with which MHD signals propagate in the lower (1.1 to 3 solar radii) corona, where metric wavelength bursts are generated, is about 400 to 500 km s^{-1}." Some metric type II bursts are known to be produced by CMEs moving with a speed of only 250 km s^{-1} (see Fig. 1 of Gopalswamy *et al.* 2001*a*), which represents a significant departure from the characteristic speed 400-500 km s^{-1}. From

in-situ observations, we know that the Alfvén speed is very low ($\sim$ 50 km s^{-1}) close to 1 AU as compared to the solar wind speed, so the latter is the primary characteristic speed in deciding shock formation. On the other hand, in the equatorial low corona ($<2\ R_\odot$) the fast magnetosonic speed (V_F, determined by the Alfvén speed V_A and the sound speed V_S) is dominant because the solar wind is not fully formed (the solar wind speed picks up at around 6 $R_\odot$). Typical V_A at the coronal base for a magnetic field of 1 G and a density of $\sim 5 \times 10^8$ cm^{-3} is $\sim$ 175 km s^{-1} while V_S is about 110 km s^{-1}, resulting in $V_F \sim$ 207 km s^{-1}. The Alfvén speed is known to have a peak in the outer corona (around 3.5 $R_\odot$) with a value of several hundred km s^{-1} (see, Krogulec *et al.* 1994; Hollweg 1978; Mann *et al.* 1999; Gopalswamy *et al.* 2001a). Clearly, drivers of moderate speed cannot form shocks in this region. In addition to this outer coronal peak, there is another peak in the inner (active region) corona because V_A could be as high as $\sim$4000 km s^{-1} (Gopalswamy *et al.* 2001a). Between these two peaks (within about 1.5 R$_\odot$), the quiet-Sun V_A dominates, resulting in a low-V_A region in the metric corona (see Fig. 15.11). We can immediately infer that a CME of modest speed (250 km s^{-1}) could drive a shock in the inner corona, while higher speeds are needed in the outer corona. In other words, it is easy for a CME to drive a shock in the inner corona, consistent with the abundant metric type II bursts and progressively smaller number of DH and kilometric type II bursts.

Mann *et al.* (1999) used the quiet-Sun Alfvén speed profile (without the AR part) to study the relation between EIT waves and metric type II bursts. They required that shocks related to metric type II bursts need to have speeds exceeding 408 km s^{-1} (corresponding to region 2 in Figure 15.11). They assumed that EIT waves and shocks were responsible for metric type II bursts from the same flare and concluded that, "a coronal shock wave must have a velocity exceeding 800 km s^{-1} in order to penetrate into the IP space." Contrary to this, Gopalswamy *et al.* (2001a) proposed the possibility of slow and accelerating CMEs driving shocks in the IP medium without a metric type II burst. In fact, the V_F profile in Figure 15.11 can explain most of the observed characteristics of metric, DH and kilometric type II bursts: (1) In the active region corona, V_F is very high, so it is difficult to form shocks. This might explain the low starting frequency of $\sim$ 150 MHz for metric type II bursts. (2) It is easy to produce metric type II bursts in the inner corona because V_F is very low (region 2 in Fig. 15.11). Only a small number of such shocks can continue beyond $\sim 3 R_\odot$. (3) A long-lived driver, such as a CME, has more opportunity to produce a type II burst because it goes through a low V_F region, especially in the outer corona. (4) CMEs with intermediate speeds can drive shocks in the metric domain, lose the shock in the regions of V_{Fmax}, and again set up a shock in the outer corona (Gopalswamy & Kaiser 2002). (5) Accelerating, low-speed CMEs may produce shocks in the DH and kilometric domains even though they do not drive

shocks in the metric domain. (6) Blast waves and shocks driven by short-lived drivers have less chance to go beyond the metric domain, unless their initial speed exceeds V_{Fmax}. No blast wave shocks have ever been observed *in situ*, although Leblanc *et al.* (2001) claimed that the blast wave and the CME-driven shock merge somewhere in the solar wind (beyond 30 $R_\odot$). Shocks observed at 1 AU without a driver (Schwenn 1996) have been shown to be flanks of shocks driven by limb CMEs (Gopalswamy *et al.* 2001a).

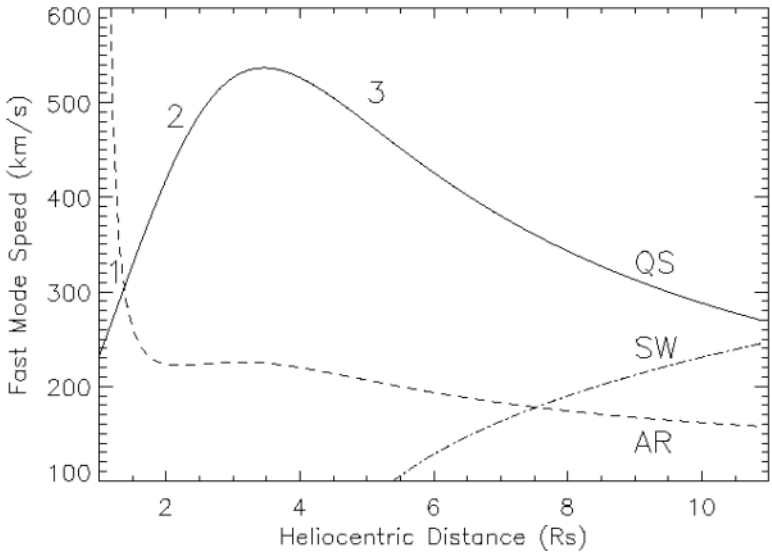

Figure 15.11. Radial profile of the fast mode speed (V_F) in the active region (AR) and quiet (QS) corona. The solar wind speed profile (SW) is also shown. The sharp increase of V_F in region 1 prevents shock formation in the core of active regions. Shock formation is easier in regions 2 and 3 because of lower V_F.

The good correlation between shock speed parameters derived from the DH type II bursts and CME plane-of-the-sky speeds (correlation coefficient = 0.71) and the lack of correlation between the shock speed parameters derived from the metric type II radio bursts and the corresponding CME speeds (correlation coefficient $= -0.07$) found by Reiner *et al.* (2001b) can be reconciled if we note that the CME speed changes rapidly in the inner corona and the CME is propagating through the region of highly variable Alfvén speed profile. Another possibility is that the metric type II bursts come from the flanks of the CME-driven shock (Holman & Pesses 1983) while the IP type II bursts come from the nose of the same shock. This would also account for the lower heliocentric distance of the type II source compared to the CME leading edge—an argument

used to discount CME-driven shock for metric type II bursts (Gopalswamy & Kundu 1992).

4. Recent Developments

In this section we discuss two IP radio signatures detected by Wind/WAVES that are closely related to the topics discussed in this chapter: (1) The radio signatures of CME interaction, and (2) long-lasting continuum at very low frequencies. These observations illustrate the complexity of the IP medium imposed by multiple solar eruptions and other large-scale structures such as coronal holes and streamers.

4.1 Radio signatures of CME interaction

Gopalswamy *et al.* (2001*c*) reported intense continuum-like radio enhancement at the low-frequency end of a DH type II burst. At the time of the radio enhancement, coronagraphic images revealed a fast (660 km s^{-1}) CME overtaking a slow (290 km s^{-1}) CME in the IP medium. The type II burst preceding the radio enhancement was due to the fast CME. The duration of the radio enhancement corresponded to the transit time of the CME-driven shock through the core of the slow CME. Exactly at the time of interaction, the core of the slow CME changed its trajectory. The radio enhancement was interpreted to be due to shock strengthening when it propagated through the dense material of the slow CME. From radio observations, Gopalswamy *et al.* (2001*c*) were able to determine the density of the core of the preceding CME to be 4×10^4 cm^{-3}, about 4 times greater than that of the ambient medium at a heliocentric distance of $6.5R_\odot$.

4.1.1 Radio signature solely due to CME interaction. In addition to the modification of a normal type II radio burst, generation of new nonthermal emission at the time of CME collision has also been found (Gopalswamy *et al.* 2002*a*). The radio emission occurred at a distance beyond $10R_\odot$ from the Sun, where the two CMEs came in contact. There was no type II radio burst (metric or IP) preceding the nonthermal emission. Using Hα and EUV images, the two CMEs were found to be ejected along the same path. The first CME was rather slow (290 km s^{-1}), while the second CME was twice as fast (590 km s^{-1}). Figure 15.12 shows the two CMEs (CME1 and CME2) in a single LASCO image. CME1 was at a heliocentric distance of $\sim 15R_\odot$, while CME2 was at a distance of $\sim 8R_\odot$. At the time of the radio burst, the leading edge of CME2 just caught up with the trailing edge of CME1 at a projected heliocentric distance of $\sim 10R_\odot$. The close temporal association between the onset of the radio burst and the time of interaction between the two white-light CMEs

suggests that the radio emission is a direct consequence of the CME interaction. CME1 was too slow to drive any shock in the outer corona due to the hump in the fast-mode speed (Gopalswamy *et al.* 2001*a*). The ability of CME2 to drive a shock is marginal because of the relatively high fast-mode speed, and increasing solar wind flow. The nonthermal electrons responsible for the new type of radio emission must have been accelerated due either to the reconnection between the two CMEs or to the formation of a new shock at the time of the collision between the two CMEs. The latter situation is a variant of the previous case, in that the shock is newly formed rather than getting a boost.

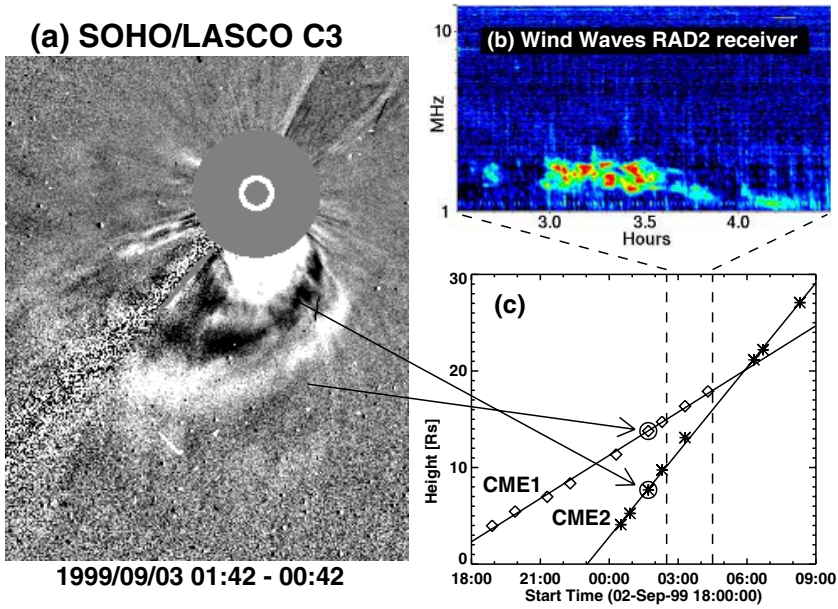

Figure 15.12. (*a*) Two CMEs on 1999 September 03 as observed by SOHO/LASCO, and (*b*) the associated continuum radio emission detected by Wind/WAVES around 2 MHz. (*c*) The height-time plots of the two CMEs with the duration of the radio emission marked by vertical lines.

4.1.2 Medium modification: Interaction between two fast CMEs.

We now discuss the interaction between two fast CMEs that occurred on 2001 January 20. The WAVES dynamic spectrum, LASCO CMEs and their height-time plots are shown in Figure 15.13. The first CME had a speed of 830 km s^{-1} and produced a narrowband type II burst with fundamental-harmonic structure. The second CME followed within two hours and was much faster (1460 km s^{-1}). Near-surface imaging data such as SOHO/EIT revealed that the two CMEs originated from the same active region (AR 9313). Note that the slow-drift type II burst following the second CME is very intense and the

bandwidth (>100%) was much larger than usual for DH type II bursts. There is no fundamental-harmonic structure. Broadband structure means that radio emission is produced from a large range of plasma level at the same time. The long decay time at a given frequency suggests that the shock traverses a given plasma level (at different spatial locations) for a long time. This situation is consistent with the shock of the second CME passing through the material of the first CME.

4.1.3 Interaction between CMEs with high but nearly equal speeds. On 2001 November 22, two CMEs lifted off from AR 9704 (S25W67) and AR 9698 (S15W34), within 3 h of each other. The two solar sources were separated by just 10° in latitude and 33° in longitude. Both were halo CMEs (their true widths are likely to greatly exceed 60°) so interaction between them is expected. The two CMEs had almost the same sky-plane speed (1443 km s^{-1} for CME1 and 1437 km s^{-1} for CME2). The two events were also associated with major flares and solar energetic particle events. The radio emission associated with the two CMEs consisted of the two standard features: a set of complex type III bursts and a type II burst. The first type II burst was close to a normal one with a band width of $\sim$ 10% (see Figure 15.14). The second type II was extremely broad band ($>$ 100%) with a complex structure. The type II burst associated with the second CMEs was spectacular, while the first type II was barely visible on the scale of the spectrum. The shock of CME1 must have propagated through a normal ambient medium while the shock driven by CME2 propagated through the material of CME1—a different ambient medium. Since both CMEs are propagating with roughly the same speed, the relative situation must have persisted for a long time (Gopalswamy *et al.* 2003a).

4.1.4 What we mean by CME interaction. The CME interaction discussed above concerns only the modification of electron acceleration in shocks. CME interactions can also take place without radio emission, especially when the interacting CMEs are slow. Near the Sun a CME is observed as a density enhancement above the ambient corona. This enhancement is thought to be the material in closed magnetic loops overlying the neutral line in the pre-eruption phase. Many CMEs have substructures such as a cavity, and a core of high-density cool material. As CMEs move away from the Sun, they expand and the density decreases. How these substructures result in the observed IP CMEs (or ICMEs) is a topic of current research (Gopalswamy 2003) For example, magnetic clouds are one type of ICME consisting of a flux rope structure. Shocks ahead of fast CMEs that catch up with slow ones might strengthen or weaken depending on the Alfvén speed (V_A) in the preceding CME because $dV_A/V_A = dB/B - 1/2\, dn_e/n_e$, where B and n_e are the mag-

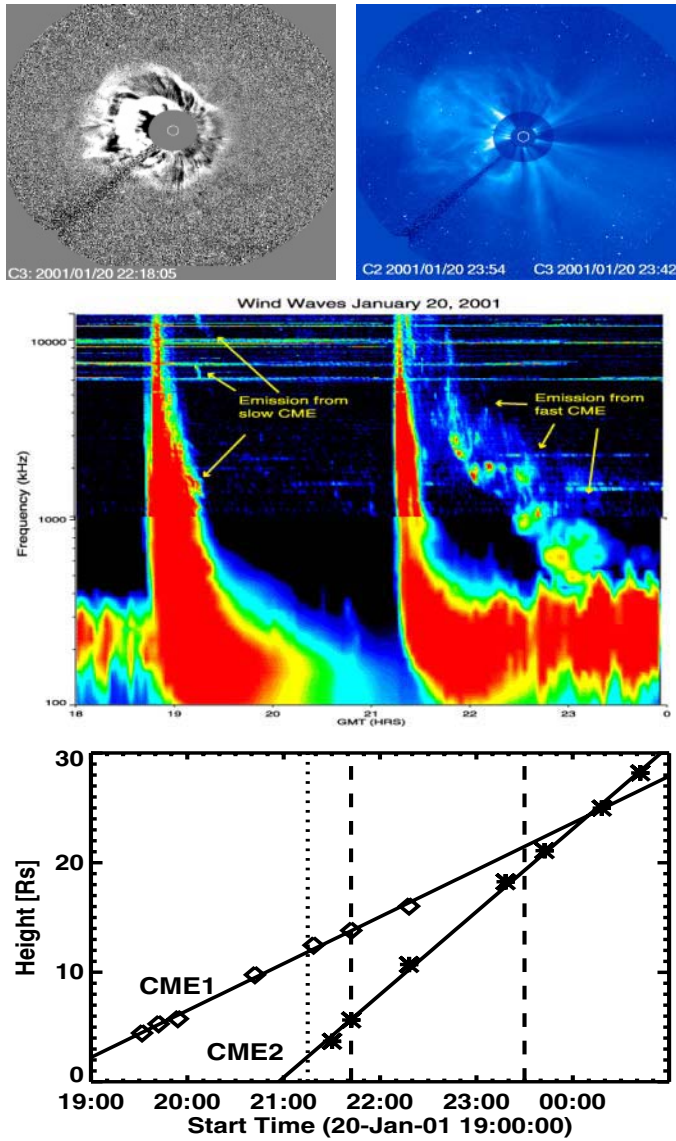

Figure 15.13. *top*: SOHO/LASCO difference image at 22:18 UT on 2001 January 20 showing two CMEs that became indistinguishable in the 23:42 UT image. *middle*: DH type II bursts associated with the two fast CMEs. The type II burst of CME1 was weak and of narrow band compared to the intense broadband type II associated with CME2. *bottom*: Height-time plots of the two CMEs with the vertical dashed lines showing the duration of the type II burst of CME2. The vertical dotted line shows the onset of the complex type III burst that mark the onset of CME2.

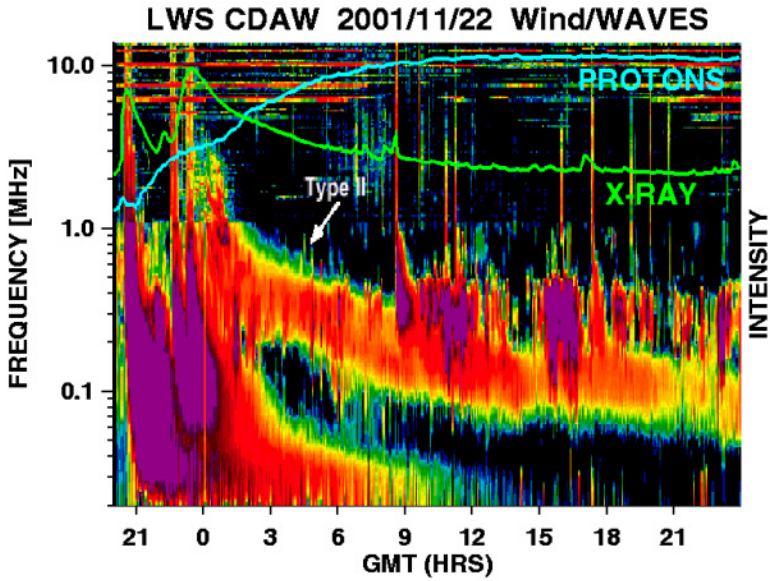

Figure 15.14. Wind/WAVES dynamic spectrum of the 2001 November 22 events. The type II burst (marked by arrow) of the second CME was intense and broadband. Both CMEs were associated with major flares as indicated by the GOES light curve (X-RAY) and the solar energetic particle time profile.

netic field and density in the preceding CME. Some numerical simulations have shown that shocks strengthen when passing through preceding CMEs (Wu *et al.* 2002; Odstrcil *et al.* 2003). Others have shown weakening of the shock, especially close to 1 AU (Vandas *et al.* 1997). Various signatures may be expected depending on the location of the interaction region between Sun and the observing spacecraft. Obviously, we cannot observe CME interactions beyond the LASCO field of view. At present, only *in-situ* observations can detect CME interactions, but by that time the CMEs will have already evolved considerably. Interaction between ICMEs have been discussed before by Burlaga *et al.* (1987). Complex extended ejecta may result due to merger of ejecta at 1 AU (Burlaga *et al.* 2002). CME interaction has important implications for space weather prediction based on halo CMEs: some of the false alarms could be accounted for by CME interactions. The observed CME interaction could also explain some of the complex ejecta at 1 AU, which have unusual composition. More work is needed to classify and recognize radio signatures for a deeper understanding of the phenomenon.

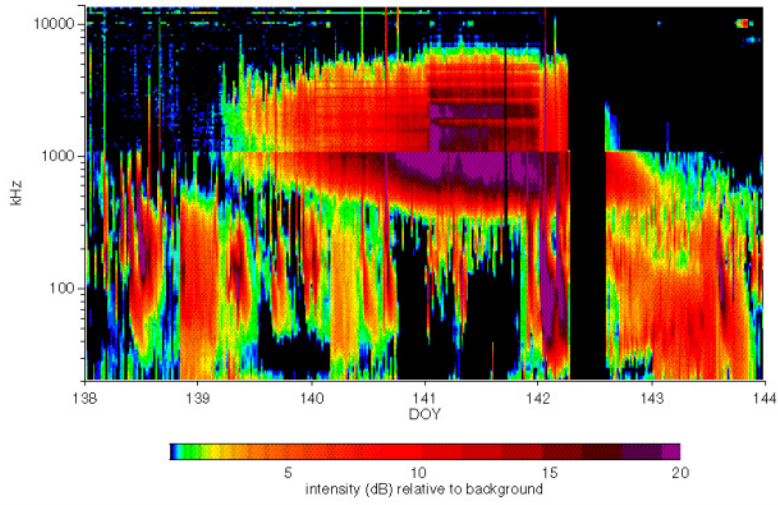

Figure 15.15. Wind/WAVES dynamic spectrum of the unusual and broadband radio emission that lasted for 4 days from 2002 May 18 (DOY 138) to May 23 (DOY 143).

4.2 Unusual radio signatures

An intense, broadband (350 kHz–7 MHz) solar radio event was observed from 2002 May 19–23 by Wind/WAVES (see Figure 15.15). The radio emission had frequency fine structures with 1.5–2 h periodicity and 100% circular polarization. The frequency spectrum has a peaked distribution, with peak frequency decreasing with time. The high frequency level remained constant, while the low frequency end drifted to lower frequencies until the middle of May 21 and remained at this level for the rest of the time (see Figure 15.15).

There was a sudden decline of the continuum at the high frequency end following two CMEs from the southwest quadrant towards the end of May 21 and beginning of May 22. The radio emission disappeared completely on May 23 at 9 UT. There was an unfortunate data gap just at the time of the onset of the decline. The direction-finding analysis reported by Reiner *et al.* (2002) indicates that the radio source may lie somewhere between 4 and 40 $R_{\odot}$ from the Sun and that the source is relatively small. Although Reiner *et al.* (2002) suggested that this could be a unique kilometric manifestation of a moving type IV burst, the high degree of polarization points to a hectometric storm continuum. A similar continuum identified by Fainberg & Stone (1970) in the RAE-1 data (0.54–2.8 MHz) was found to be related to decametric and metric

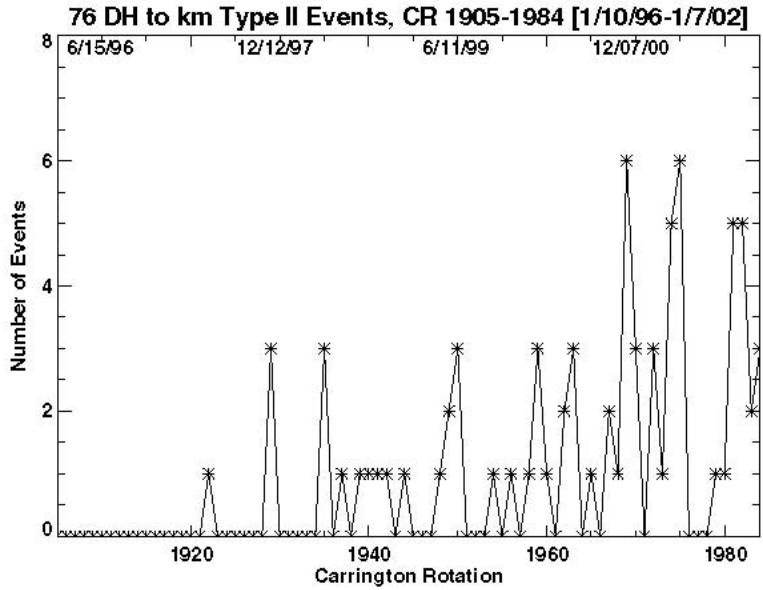

Figure 15.16. Number of type II bursts that begin in the DH domain and continue to the kilometric domain plotted as a function of time (Carrington Rotation number and UT). Note that there are several rotations with no such long-lasting type II bursts.

noise storms (Sakurai 1976). When we examined the solar disk, we found that the onset of the continuum coincided with the appearance of a rapidly changing active region complex (AR 9957 and 9958) located at the edge of an equatorial coronal hole. When continuum started, AR 9957 was at N14E45 and at N10W15 when it ended. The number of sunspots and the active region area were growing rapidly and reached maximum around May 21-22. The radio event disappeared when the active region area dropped to the pre-burst value on May 23. The sunspot number declined at a slightly lower rate.

5. Concluding Remarks

Research on IP radio bursts started in the sixties and tremendous progress has been made, thanks to the series of space missions with radio instruments on board. While early studies concentrated on the radio phenomenon in isolation, connecting them to solar disturbances started in the eighties. We now see that the complex type III bursts and type II bursts are intimately connected to CMEs. This has opened up new opportunities to study the propagation of CME-related disturbances far into the IP medium because radio emission can be observed over the whole Sun-Earth connected space and beyond. These two burst types

also serve as proxies to the two commonly accepted sources of solar energetic particles: flare reconnection and shocks. The simple picture of CMEs and shocks propagating through a plain solar wind may not happen all the time, especially during solar maximum.

With the CME rate averaging to more than 5 per day, the IP medium is expected to be highly disturbed whenever CMEs are ejected in rapid succession from the same region. The radio signatures during CME interaction have opened a new avenue to study the disturbed IP medium. Between 1996 and 2002, SOHO/LASCO detected nearly 7000 CMEs. Yet, there were only about 600 metric type II bursts and about 300 IP type II bursts. Out of the latter 300, only 76 produced radio emission over the entire stretch of the Sun-Earth space (see Figure 15.16). Most of them were also associated with major SEP events. Thus, the IP type II bursts provide unique information on geo-effective CMEs. We were able to make tremendous progress using radio observations with little positional information. Imaging the complex type III bursts, IP type II bursts and the interaction signatures from space is a logical next step to get direct information on shocks and electron beams. Such a possibility with the Solar Imaging Radio Array (SIRA) is within our reach. With the anticipated synergistic contributions from LOFAR and FASR on the ground, solar radio astronomy is poised for a leap.

Acknowledgments

I thank S. Yashiro, A. Lara, and S. Nunes for help with figures and M. J. Reiner, P. K. Manoharan, and S. Nunes for a critical reading of the manuscript.

References

Alexander, J. K., Malitson, H. H. & Stone, R. G., 1969, Solar Phys., 8, 388

Aubier, M. G., Leblanc, Y. & Moller-Pederson, B., 1978, A&Ap, 70, 685

Bale, S. D. and Reiner, M. J. and Bougeret, J.-L. and Kaiser, M. L. and Krucker, S. and Larson, D. E. and Lin, R. P. 1999, GRL, 26, 1573

Boishot, A., de la Noe, J. & B. Moller-Pederson, 1970, A&Ap, 4, 159

Boischot, A., Riddle, A. C., Pearce. J. B., & Warwick, J. W., 1980, Solar Phys., 5, 397

Bougeret, J.-L., Fainberg, J., & Stone, R. G., 1984, A&Ap, 141, 17

Bougeret, J.-L., Kaiser, M. L., Kellogg, P. J., Manning, R., Goetz, K., Monson, S. J., Monge, N., Friel, L., Meetre, C. A., Perche, C., Sitruk, L. & Hoang, S. 1995, Space Sci. Rev., 71, 231

Bougeret, J.-L., Zarka, P., Caroubalos, C., Karlický, M., Leblanc, Y., Maroulis, D., Hillaris, A., Moussas, X., Alissandrakis, C. E., Dumas, G. & Perche, C. 1998, GRL, 25, 2513

Brueckner, G.E. *et al.* 1995, Solar Phys., 162, 357

Burlaga, L. F., Behannon, K. W. & Klein, L. W. 1987, JGR, 92, 5725
Burlaga, L. F., Plunkett, S. P. & St. Cyr, O. C. 2002, JGR, 107, A10, SSH 1-1
Cane, H. V., Stone, R. G., Fainberg, J., Steinberg, J. L., Hoang, S. & Stewart, R. T. 1981, GRL, 8, 1285
Cane, H. V., 1983, Solar Wind Five, NASA Conf. Publ., CP-2280, 703
Cane, H. V. & Stone, R. G., 1984, ApJ, 282, 339
Cane, H. V., Sheeley, N. R. & Howard, R. A. 1987, JGR, 92, 9869
Cane, H. V., Erickson, W. C. & Prestage, N. 2002, JGR, 107, A10
Cliver, E. W., Webb, D. F. & Howard, R. A. 1999, Solar Phys., 187, 89
Dulk, G. A., Leblanc, Y., Robinson, P. A., Bougeret, J. & Lin, R. P. 1998, JGR, 103, 17223
Elgaroy, O. 1977, Solar Noise Storms, Pergamon, New York
Fainberg, J. & Stone, R. G. 1970, Solar Phys., 15, 433
Fainberg, J. & Stone, R. G. 1971, Solar Phys., 17, 392
Fainberg, J., Evans, R. G. & Stone, R. G. 1972, ApJ, 178, 743
Fitzenreiter, R., Evans, R. G. & Lin. R. P. 1976, Solar Phys., 46, 437
Fitzenreiter, R. J., Fainberg, J., Weber, R. R., Alvarez, H., Haddock, F. T. & Potter, W. H. 1977, Solar Phys., 52, 477
Gary, D. E., Dulk, G. A., House, L., Illing, R., Sawyer, C., Wagner, W. J., McLean, D. J. & Hildner, E. 1984, A&A, 134, 222
Ginzbursg, V. L. & Zheleznakov, V., V. 1958, Soviet Astron. A. J. 2, 653
Gopalswamy, N. 2000, in Radio Astronomy at Long Wavelengths, Geophysical Monograph 119, AGU, Washington DC, 123
Gopalswamy, N. 2003, Adv. Space Res., 31(4), 869
Gopalswamy, N. & Kundu, M. R. 1992, in AIP Conference Proceedings # 264: Particle Acceleration in Cosmic Plasmas, ed. by G. P. Zank & T. K. Gaisser, American Institute of Physics, New York, 257
Gopalswamy, N., Kaiser, M. L., Lepping, R. P., Kahler, S. W., Ogilvie, K., Berdichevsky, D., Kondo, T., Isobe, T. & Akioka, M. 1998, JGR, 103, 307
Gopalswamy, N., Kaiser, M. L., Thompson, B. J., Burlaga, L. F., Szabo, A., Vourlidas, A., Lara, A., Yashiro, S. & Bougeret, J.-L. 2000, GRL, 27, 1427
Gopalswamy, N., Lara, A., Kaiser, M. L. & Bougeret, J.-L. 2001a, JGR, 106, 25261
Gopalswamy, N., Yashiro, S., Kaiser, M. L., Howard, R. A. & Bougeret, J.-L. 2001b, JGR, 106, 29219
Gopalswamy, N. & Kaiser, M. L. 2002, Adv. Space Res. 29, 307
Gopalswamy, N., Yashiro, S., Kaiser, M. L., Howard, R. A. & Bougeret, J.-L. 2001c, ApJ, 548, L91
Gopalswamy, N. *et al.* 2003a, GRL, 30, No. 12, 8015
Gopalswamy, N. *et al.* 2003b, in Solar Wind X, ed. M. Velli, in press
Gosling, J. T., Hildner, E., MacQueen, R. M., Munro, R. H., Poland, A. I. & Ross, C. L. 1976, Solar Phys., 48, 389

Hartz, T. R. 1964, Ann. Astrophys. 27, 831
Hartz, T. R. 1969, Planetary Space Sci., 7, 267
Hartz, T. R. & Gradel, T. E. 1970, ApJ, 160, 293
Holman, G. D. & Pesses, M. E. 1983, ApJ, 267 837
Hollweg, J. V. 1978, Solar Phys. 56, 305
Kahler, S. W., Sheeley, N. R., Howard, R. A., Michels, D. J. & Koomen, M. J. 1984, Solar Phys., 93, 133
Kahler, S. W., Cliver, E. W. & Cane, H. V. 1986, Adv. Space Res., 6(6), 319
Kaiser, M. L., 2003, Adv. Space Res., in press
Kaiser, M. L., Reiner, M. J., Gopalswamy, N., Howard, R. A., St. Cyr, O. C., Thompson, B. J. & Bougeret, J.-L. 1998, GRL, 25, 2501
Klassen, A., Bothmer, V., Mann, G., Reiner, M. J., Krucker, S., Vourlidas, A. & Kunow, H. 2002, A&A, 385, 1078
Klein, K.-L. 1995, in Coronal Magnetic Energy Releases, Lecture Notes in Physics, volume 444, 55
Knock, S. A., Cairns, I. H., Robinson, P. A. & Kuncic, Z. 2003, JGR, 108 (A3), SSH 6-1
Krogulec, M., Musielak, Z. E., Suess, S. T., Nerney, S. F. & Moore, R. L. 1994, JGR, 99, 23489
Kundu, M. R. & Stone, R. G. 1984 Adv. Space Res., 4, 261
Lara, A., Gopalswamy, N., Nunes, S., Muñoz, G. & Yashiro, S. 2003, GRL, 30, No.12, SEP 4-1
Leblanc, Y., Dulk, G. A., Cairns, I. H. & Bougeret, J.-L. 2000, JGR, 105, 18215.
Lengyel-Frey, D. & Stone, R. G. 1989, JGR, 94, 159
Lin, R. P., Evans, R. G. & Fainberg, J. 1973, Astrophys. Lett. & Comm., 14, 191
MacDowall, R. J., Stone, R. G. & Kundu, M. R. 1987, Solar Phys., 111, 397
MacDowall, R. J., Lara, A., Manoharan, P. K., Nitta, N. V., Rosas, A. M. & Bougeret, J. L. 2003, GRL, 30, No. 12, SEP 6-1
Malitson, H. H., Fainberg, J., & Stone, R. G., 1973 Observation of a Type II Solar Radio Burst to 37 Rsun, Astrophys. Lett., 14, 111
Mann, G., Klassen, A., Estel, C. & Thompson, B. J. 1999, in Proc. of 8th SOHO Workshop, Edited by J.-C. Vial & B. Kaldeich-Schmann., p.477
Moller-Pederson, B. 1974, A&A, 37, 163
Nelson, G. J. & Melrose, D. B. 1985, in Solar Radio Physics, edited by D. J. McLean & N. R. Labrum, Cambridge, New York, p. 333
Odstrcil, D., Vandas, M. & Pizzo, V. 2003, Solar Wind 10, in press
Payne-Scott, R., Yabsley D. E. & Bolton, J. G. 1947, Nature, 160, 256
Reames, D. V., Ramaty, R. & von Rosenvinge, T. T. 1988, ApJ, 332, L87
Reiner, M. J., Kaiser, M. L. & Fainberg, J. 1998, JGR, 103, 29651
Reiner, M. J. & Kaiser, M. L. 1999, JGR, 104, 16979

Reiner, M. J., Karlický, M., Jiricka, K., Aurass, H., Mann, G. & Kaiser, M. L. 2000, ApJ, 530, 1049

Reiner, M. J., Kaiser, M. L., Karlický, M., Jiricka, K. & Bougeret, J.-L. 2001a, Solar Phys., 204, 121

Reiner, M. J., Kaiser, M. L., Gopalswamy, N., Aurass, H., Mann, G., Vourlidas, A. & Maksimovic, M. 2001b, JGR, 106, 25279

Reiner, M. J., Kaiser, M. L. & Fainberg, J. 2002, AGU Fall Meeting 2002, abstract #SH72C-02

Robinson, R. D., Stewart, R. T. & Cane, H. V. 1984, Solar Phys., 91, 159

Schwenn, R. 1996, Astrophys. Space Sci., 243, 187

Sakurai, K. 1976, Astrophys. Space Sci., 42, 349

Sheeley, N. R., Jr., Howard, R. A., Michels, D. J., Koomen, M. J., Schwenn, R., Muehlhaeuser, K. H. & Rosenbauer, H. 1985, JGR, 90, 163

Slysh, V. I. 1967a, Soviet Astron. 11, 389

Slysh, V. I. 1967b, Cosmic Res., 5, 759

Stewart, R. T. & Labrum, N. R. 1972, Solar Phys., 27, 192

Stone, R. G., Weiler, K. W., Goldstein, M. L. & Bougeret, J.-L. 2000, Radio astronomy at long wavelengths, AGU, Washington, DC

Uchida, Y. 1960, PASJ, 12, 376

Uchida, Y. 1974, Solar Phys., 39, 431

Vandas, M. Fischer, S., Dryer, M., Smith, Z., Detman, T. & Geranios, A. 1997, JGR, 102, 22295

Wagner, W. J. & MacQueen, R. M. 1983, A&Ap, 120, 136

Wild, J. P. 1950, Aust. J. Sci. Ser. A, 3, 541

Wild, J. P. & McCready, L. L. 1950, Austral. J. Sci. Res., A3, 387

Wild, J. P. & Smerd, S. F. 1972, Ann. Rev. Astron. Astrophys., 10, 159

Wu, S. T., Wang, A. H. & Gopalswamy, N. 2002, in SOLMAG 2002, Ed. H. Sawaya-Lacoste, ESA SP-505. Noordwijk, Netherlands, p. 227